Nanoscale

PAPER

View Article Online
View Journal | View Issue

Cite this: *Nanoscale*, 2024, **16**, 6309

Magnetotransport spectroscopy of electroburnt graphene nanojunctions†

Zhengyang Jin,‡[a] Caigan Xi,‡[a] Jun Chen,*[a] Yiping Ouyang,[a] Feng Wang,[a] Minhao Zhang *[a,b] and Fengqi Song [a,b]

Received 3rd December 2023,
Accepted 26th February 2024

DOI: 10.1039/d3nr06176k

rsc.li/nanoscale

We have reported the precise methodology for fabricating graphene quantum dots through electroburning and performed measurements on the Coulomb blockade and oscillation phenomena. The diameters of graphene quantum dots can be estimated to range from several to tens of nanometers, utilizing the disk capacitance model and the two-dimensional quantum well model. By subjecting the quantum dots to a vertical magnetic field, an obvious alteration in conductance can be detected at the point of resonance tunneling. This observed phenomenon can be attributed to the modification in the density of states of Landau levels within the graphene leads. Moreover, by manipulating the gate voltage, it is possible to regulate the Fermi level of the lead, resulting in distinct magnetoresistance of different electron states. The presence of this lead effect may potentially disrupt the magnetic response analysis of graphene-based single-molecule transistors, necessitating a comprehensive theoretical examination to mitigate such interference.

Since the isolation and subsequent discovery of graphene through mechanical stripping from highly oriented pyrolytic graphite,[1] extensive research has been conducted on the quantum effect exhibited by this two-dimensional material.[2–4] Owing to its hexagonal lattice structure, graphene possesses exceptional electrical conductivity and temperature stability, which lay a solid foundation for the development and application of novel electronic devices in the future.[5]

Various specialized processes have been employed to treat graphene, including the controlled electroburning method which generates a nanoscale gap in graphene nanoribbons.[6–9] These gaps are exploited to fabricate single-molecule transistors by introducing molecules into them.[10,11] The organic chain molecules with multiple benzene rings at their ends are capable of forming π–π coupling with graphene leads on both sides of the gap,[12–17] while chain molecules featuring an amino group at their ends can form covalent bonds with the carboxyl group located at the ends of the graphene gap.[18–20]

There exists a unique case where graphene quantum dots are present in the nanogap formed through the electroburning method.[21] These quantum dots exhibit electrical transport properties highly similar to those of single-electron transistors; for instance, both exhibit the Coulomb blockade phenomenon.[22] Moreover, the blocking region exhibits a significant addition energy,[23] ensuring that this characteristic is maintained even at room temperature. Additionally, by applying a top gate voltage,[24–27] quantum dots can be isolated within specific regions of flake graphene. Notably, graphene quantum dots also demonstrate peculiar fluorescence phenomena and possess immense potential in future applications such as bioimaging, sensors, catalysts, and optoelectronic devices.[28] However, further investigation is necessary to fully understand the electrical transport properties of graphene quantum dots and their response to applied magnetic fields.

In this study, we present a novel approach for the fabrication of graphene quantum dots. Initially, a single layer of graphene synthesized through chemical vapor deposition (CVD) is carefully transferred onto a 300 nm silicon oxide substrate. Subsequently, a 500 nm wide graphene ribbon is precisely patterned using electron beam lithography and oxygen plasma etching techniques. The Raman spectrum analysis of the employed monolayer graphene is presented in Fig. 1a. Furthermore, to serve as the source and drain electrode, we utilize a well-defined 20 nm Cr/200 nm Au pad patterned on the graphene surface while employing highly doped conductive silicon as the back gate electrode.

We employ a feedback-controlled electroburning program to fracture the graphene ribbon under ambient conditions at room temperature. A voltage ramp of 1 V s^{-1} is applied to the

[a]*National Laboratory of Solid State Microstructures, Collaborative Innovation Center of Advanced Microstructures, and School of Physics, Nanjing University, Nanjing 210093, China. E-mail: dz1922001@smail.nju.edu.cn, zhangminhao@nju.edu.cn*
[b]*Atom Manufacturing Institute (AMI), Nanjing 211805, China*
†Electronic supplementary information (ESI) available. See DOI: https://doi.org/10.1039/d3nr06176k
‡These authors contributed equally to this work.

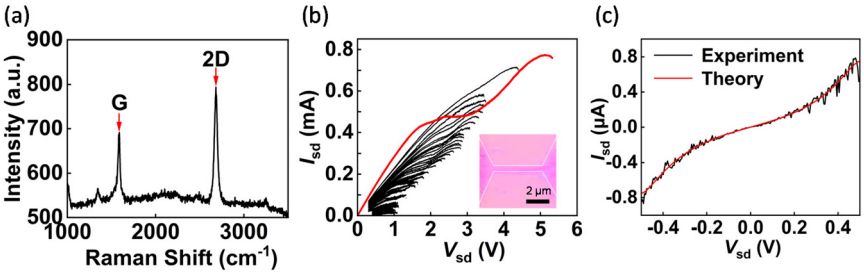

Fig. 1 Graphene quantum dot devices fabricated by electroburning. (a) Standard Raman diagram of a single-layer graphene; compared with G peaks, the higher 2D peaks show a monolayer characteristic. (b) *I*–*V* curves of the feedback electroburning process; the red line is the curve of the first cycle, and the illustration is the graphene nanoribbon diagram under a microscope. (c) *I*–*V* curve after electroburning, obtained using the Simmons model to estimate the gap at 1–2 nm.

source electrode, while monitoring and recording real-time current as well as maximum current during the process. Upon detection of a decrease in real-time current, the voltage is rapidly ramped down to 0 V within 1 ms. The feedback condition is adjusted based on the previous feedback threshold voltage. This iterative program continues until the low bias resistance between the source and drain electrodes exceeds 100 MΩ. Fig. 1b illustrates the source–drain current–voltage (*I*–*V*) curves obtained from this feedback process, where the red curve represents the *I*–*V* curve of the initial feedback breakage event. The inflection point of the red curve is related to the process of graphene annealing and impurity removal in an oxygen environment.[29]

The electroburning process culminates in the formation of gaps within the graphene ribbons, whose sizes are estimated using the Simmons model as depicted in Fig. 1c.[30] Most of these gaps vary in size from 1 to 2 nm and may potentially contain graphene quantum dots. By comparing current maps as a function of source–drain voltage and gate voltage at 2 K temperature in a vacuum environment, these devices can be broadly classified into four groups.[29] Fig. 2a illustrates the transport properties of the nanogap without graphene quantum dots. The current map does not exhibit any discernible pattern, while the output characteristic curve shown in Fig. 2e (with a gate voltage of −2 V) demonstrates high symmetry that can be fitted using the Simmons model. Additionally, no prominent peak is observed in the transfer characteristic curve at a bias of −2 mV, as presented in Fig. 2i.

Fig. 2b illustrates the transport characteristics of a single graphene quantum dot within the nanogap. The current map exhibits a series of discernible rhombic blocking regions, characterized by equal slopes along their corresponding edges, commonly referred to as Coulomb diamonds.[31] Under high bias conditions, electrons can traverse the boundaries of these Coulomb diamonds and enter the conduction region, resulting in an abrupt surge in current at specific bias voltages. Consequently, fitting the output characteristic curve at −2 V, as shown in Fig. 2f, using the Simmons model becomes challenging due to its deviation from the expected behaviour. Furthermore, the transfer characteristic curve at a bias of −2 mV in Fig. 2j exhibits a set of Coulomb peaks.

In Fig. 2c, the transport characteristics of multiple quantum dots within the graphene nanogap are depicted, revealing several sets of indistinguishable Coulomb diamonds with varying slopes. These diamonds correspond to abrupt points observed in the output characteristic curve at a gate voltage of −2 V in Fig. 2g and prove challenging to fit using the Simmons model. Additionally, multiple peaks can be observed in the transfer characteristic curve at a bias of −2 mV in Fig. 2k.

Fig. 2d illustrates the transport characteristics of graphene nanoribbons in a partially broken state, where multiple Coulomb diamonds are challenging to discern. In comparison with Fig. 2b and c, the size of the Coulomb diamonds is smaller while the current at both ends of the source and drain under identical bias voltage is larger. Notably, at a bias of −2 mV, Fig. 2l exhibits a transfer characteristic curve with more densely distributed peaks. The primary focus of this study is on the scenario depicted in Fig. 2b, specifically highlighting the presence of one quantum dot within the gap region.

Fig. 3 illustrates the differential conductance maps of four distinct graphene quantum dot devices under varying bias and gate voltages. The size estimation of a quantum dot can be achieved by analyzing the slopes and sizes of the Coulomb diamonds.[32] The slopes of the diamond boundaries are determined using the ratio of the capacitances to the source (C_s), drain (C_d) and gate (C_g). The positive slopes $\alpha^+ = C_g/(C_g + C_d)$ correspond to the case when the energy level of the quantum dot is aligned with the source. The negative slopes $\alpha^- = C_g/(C_s)$ correspond to the case when the energy level of the quantum dot is aligned with the drain. Taking device A as an example, which is depicted in Fig. 3a, there are three complete Coulomb diamond regions within the gate voltage range from −50 V to 50 V. Notably, these three Coulomb diamonds possess identical absolute values for their slopes (α). When $\alpha^+ = -\alpha^- = 0.018$, it is concluded that the gate coupling parameter $\beta = \dfrac{\alpha^+|\alpha^-|}{\alpha^+ + |\alpha^-|} = 0.009$, which indicates the ability of the gate to regulate the energy level of the quantum dot. The height of the Coulomb diamond in V_{sd} multiplied by one electron charge (e) represents the energy required for adding a single electron to

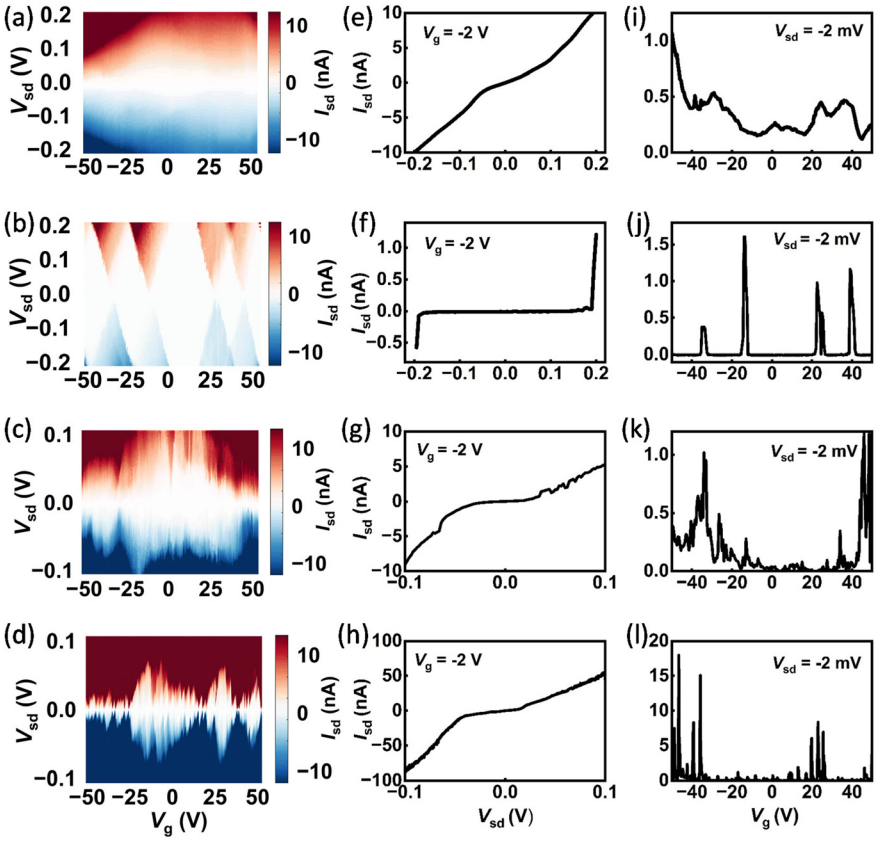

Fig. 2 Four situations of graphene nanojunctions after electroburning. (a), (b), (c) and (d), respectively, show the differential conductance of the four types of graphene after electroburning. (a) No quantum dots in the graphene nanogap. (b) One quantum dot in the gap. (c) Multiple quantum dots in the gap. (d) The graphene ribbon is not completely broken. (e), (f), (g) and (h) show the output characteristic curves corresponding to the gate voltage of −2 V in the four cases, respectively; (i), (j), (k) and (l) show the transfer characteristic curves corresponding to the four cases when the bias is −2 mV.

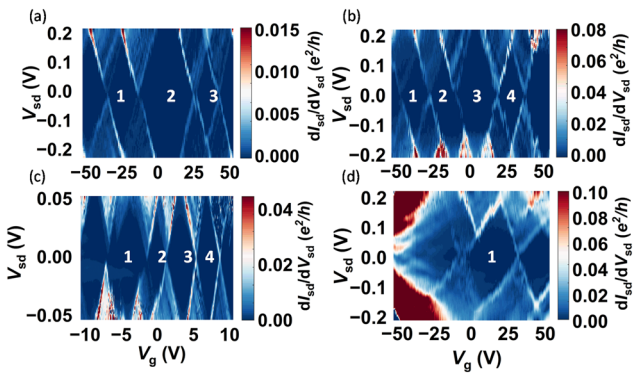

Fig. 3 Differential conductance maps of graphene quantum dots with different sizes. (a), (b), (c) and (d) show the differential conductance of devices A, B, C and D, respectively.

the quantum dot. This energy is commonly referred to as the addition energy (E_{add}). The addition energy can be divided into two components: first, the charge energy $E_c = e^2/2C$ which accounts for overcoming the repulsion between charges within the quantum dot, where $C = C_s + C_d + C_g$ is the total capacitance of the quantum dot, and second, ΔE, which denotes the difference in energy levels between the newly added electron and its predecessor. The size of the quantum dot can be estimated using two different methods with two kinds of energies. The E_{add} values for the three Coulomb diamonds in Fig. 2a are 160 meV, 300 meV, and 140 meV, respectively. In this study, we assume a constant charging energy and consider multiple degenerate states within each energy level. Consequently, it can be inferred that a Coulomb diamond exhibiting a higher addition energy indicates electron occupation at an elevated energy level. Conversely, a Coulomb diamond with lower addition energy suggests electron filling in different degenerate states within the same energy level. The minimum E_{add} = 140 meV is taken as the charging energy E_c to calculate the total capacitance of the quantum dot as $C = e^2/2E_c = 0.57$ aF. The disk capacitance model was used to estimate the diameter of the graphene quantum dot $d_c = C/2(\varepsilon_0(\varepsilon_{oxide} + \varepsilon_{air}))$,[33] where ε_{oxide} = 3.9 and ε_{air} = 1. The calculated result is 6.5 nm. In addition, the maximum E_{add} = 300 meV minus the minimum E_{add} = 140 meV can be defined as the energy level spacing ΔE = 160 meV, and $d_w = h\nu_F/2\Delta E$ = 13.7 nm can be estimated by using the two-dimensional quantum well model,[23] where the

Fermi velocity $v_F = 10^6$ m s^{-1}. Both of these estimation methods show that the diameter of the quantum dot in device A quantum dot is about 10 nm.

The relevant parameters of four different devices A, B, C and D are listed in Table 1. It can be seen that the gate coupling parameters of the four devices are all within the range of 0.01 ± 0.005, which reflects that the degree of adhesion between graphene quantum dots and silicon oxide substrates is relatively uniform to a certain extent. Due to the limitation of measurement conditions, there is only one complete Coulomb diamond, it is therefore impossible to judge the specific electron filling of quantum dot D, and the E_{add} of the Coulomb diamond is regarded as E_c. The absolute values of the positive and negative slopes of device D are different, which indicates the asymmetry of electron transport between the source and drain.

Compared with the sizes of the devices A, B and D (about 10 nm), the differential conductance map of device C shows smaller Coulomb diamonds and correspondingly a larger quantum dot. This phenomenon shows that the larger the size of the quantum dot, the smaller the repulsion of the internal electrons, and therefore the smaller the addition energy required to add an electron to the quantum dot. At the same time, the increase of quantum dot size makes the energy level spacing decrease, which is consistent with the transformation law from the energy level of microscopic molecules to the energy band of macroscopic objects.

By applying a perpendicular magnetic field to the graphene dot at a bias of 2 mV, we observed anomalous changes in conductance at the point of resonance tunneling. These changes exhibit high repeatability, effectively eliminating the impact of thermal and electrical noise. We measured the 0–8 T magnetic response curves of each Coulomb peak in device C (Fig. 4a–e), revealing that each peak displays distinct responses while changing the magnetic fields. However, there are no significant changes in the central position of the peak, ruling out any Zeeman effect caused by intrinsic magnetic moments of quantum dots.[34] We attribute this unusual magnetic response to the fluctuation of density of states of the graphene leads caused by both applied electrical and magnetic fields.[35]

As a unique two-dimensional material, graphene exhibits quantized energy levels under strong magnetic fields, resulting in the formation of Landau levels as depicted in Fig. 4f.[36,37]

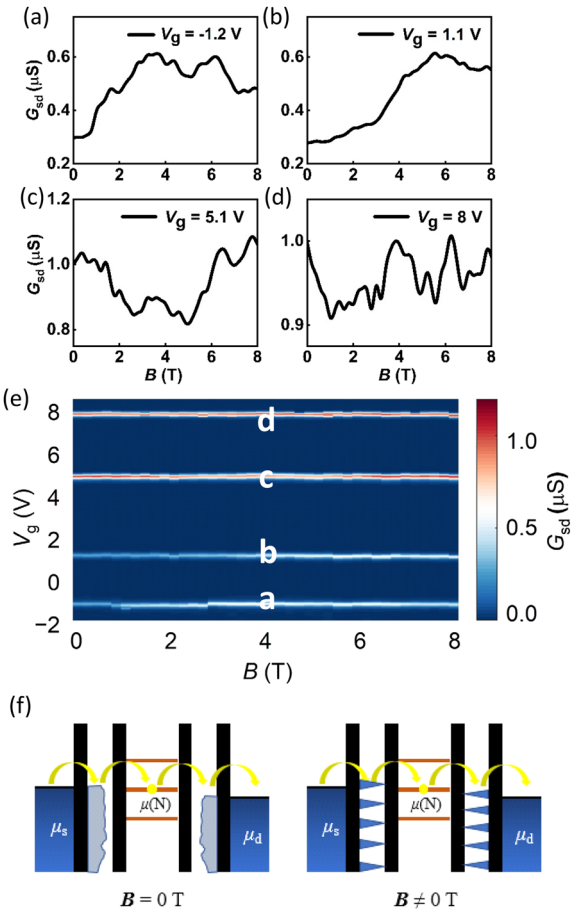

Fig. 4 Conductance change of device C in a magnetic field. (a), (b), (c) and (d) show the conductance and applied vertical magnetic field relationship of device C. The bias voltage is 2 mV, the magnetic field range is 0 to 8 T, and the gate voltage is –1.2 V, 1.1 V, 5.1 V, and 8 V, respectively. (e) The variation of the current of device C at the four Coulomb peak with the magnetic field, ranging from 0 to 8 T. (f) Schematic diagram showing magnetoconductance changes of graphene quantum dots. The leads at both ends of graphene quantum dots form Landau energy levels in magnetic fields, and the density of states changes.

The Landau level energy of the zero-mass Dirac fermion in graphene is as follows:[3]

$$E_N = \mathrm{sgn}(N)\sqrt{2e\hbar v_F^2|N|B} \quad (1)$$

Table 1 Comparison of parameters of the four devices

Device Number	α^+	α^-	β	E_c (meV)	ΔE (meV)	C (aF)	d_c (nm)	d_w (nm)
A	0.018	−0.018	0.009	140	160	0.57	6.5	13.7
B	0.02	−0.02	0.01	130	120	0.6	6.7	17
C	0.03	−0.03	0.015	40	50	2	22	41
D	0.0077	−0.015	0.005	170	—	0.47	5.3	—

The information includes the following: the device number; the positive slope of the Coulomb diamond: α^+; the negative slope of the Coulomb diamond: α^-; the gate coupling coefficient: β; the charge energy: E_c; the energy level spacing: ΔE; the total capacitance of the quantum dot: C; the diameter of the graphene quantum dot estimated with the disk capacitance model: d_c; the diameter of the graphene quantum dot estimated with the two-dimensional quantum well model: d_w.

where the integer N represents an electron-like ($N > 0$) or a hole-like ($N < 0$) Landau level index, which can be regulated using the gate voltage. As a result, the application of a large perpendicular magnetic field should induce alterations in the density of states at the Fermi surface of the graphene leads, while different gate voltages exhibit distinct magnetic responses.[38]

To illustrate the relationship between the density of states of the leads and the conductance, the current through a certain energy level orbital of a quantum dot is given by the Landau equation[35]

$$I = \frac{2e}{h}\int \mathrm{d}E T(E)[f_{\mathrm{L}}(E) - f_{\mathrm{R}}(E)] \quad (2)$$

where $f_{\mathrm{L}}(E)$ and $f_{\mathrm{R}}(E)$ denote the Fermi distribution of the graphene leads, which remain constant at a fixed bias voltage. $T(E)$ is the transmission function which is given by the Breit–Wigner formula[29]

$$T(E) = \frac{4\Gamma_{\mathrm{L}}\Gamma_{\mathrm{R}}}{[E-\varepsilon]^2 + (\Gamma_{\mathrm{L}} + \Gamma_{\mathrm{R}})^2} \quad (3)$$

where ε is the energy of the quantum dot level, and Γ_{L} and Γ_{R} characterize the quantum dot coupling to the leads, which are proportional to the density of states at the graphene leads.[35] Therefore, when the density of states changes with the magnetic field, the coupling between the quantum dot and the graphene lead also changes, causing an overall change in the transmission function and consequently impacting the total conductance at the point of resonance tunneling. Furthermore, it should be acknowledged that due to the inherent complexity within mesoscopic systems, additional effects such as weak localization arising from quantum coherence cannot be disregarded.[39–41]

In conclusion, we present a detailed procedure for synthesizing graphene quantum dots through electroburning and investigate the Coulomb blockade phenomenon at low temperatures. By employing the disk capacitance model and two-dimensional quantum well model, we estimate the diameters of various quantum dots, which range from a few to tens of nanometers. Furthermore, upon applying a vertical magnetic field, we observe significant changes in conductance attributed to variations in the Landau level within the graphene leads located at both ends of the quantum dot at the Fermi surface. Notably, adjusting the gate voltage allows for the regulation of the Fermi level within these leads, resulting in distinct conductance trends. It is crucial to acknowledge that this lead effect may potentially interfere with future analyses involving magnetic responses in graphene-based single-molecule transistors, thus necessitating comprehensive theoretical investigations aimed at mitigating such interference.

Conflicts of interest

There are no conflicts to declare.

Acknowledgements

We acknowledge the financial support of the National Key R&D Program of China (Grant no. 2022YFA1402), the National Natural Science Foundation of China (Grant no. 92161201, T2221003, 12104221, 12104220, 12274208, 12025404 and 91961101), and the Fundamental Research Funds for the Central Universities (Grant no. 020414380192).

References

1 K. S. Novoselov, A. K. Geim, S. V. Morozov, *et al.*, Electric Field Effect in Atomically Thin Carbon Films, *Science*, 2004, **306**(5696), 666–669.
2 A. K. Geim and K. S. Novoselov, The rise of graphene, *Nat. Mater.*, 2007, **6**(3), 183–191.
3 Y. Zhang, Y.-W. Tan, H. L. Stormer, *et al.*, Experimental observation of the quantum Hall effect and Berry's phase in graphene, *Nature*, 2005, **438**(7065), 201–204.
4 A. F. Young and P. Kim, Quantum interference and Klein tunnelling in graphene heterojunctions, *Nat. Phys.*, 2009, **5**(3), 222–226.
5 K. Kim, J.-Y. Choi, T. Kim, *et al.*, A role for graphene in silicon-based semiconductor devices, *Nature*, 2011, **479**(7373), 338–344.
6 F. Prins, A. Barreiro, J. W. Ruitenberg, *et al.*, Room-Temperature Gating of Molecular Junctions Using Few-Layer Graphene Nanogap Electrodes, *Nano Lett.*, 2011, **11**(11), 4607–4611.
7 C. S. Lau, J. A. Mol, J. H. Warner, *et al.*, Nanoscale control of graphene electrodes, *Phys. Chem. Chem. Phys.*, 2014, **16**(38), 20398–20401.
8 H. Sadeghi, J. A. Mol, C. S. Lau, *et al.*, Conductance enlargement in picoscale electroburnt graphene nanojunctions, *Proc. Natl. Acad. Sci. U. S. A.*, 2015, **112**(9), 2658–2663.
9 P. Gehring, H. Sadeghi, S. Sangtarash, *et al.*, Quantum Interference in Graphene Nanoconstrictions, *Nano Lett.*, 2016, **16**(7), 4210–4216.
10 J. O. Island, A. Holovchenko, M. Koole, *et al.*, Fabrication of hybrid molecular devices using multi-layer graphene break junctions, *J. Phys.: Condens. Matter*, 2014, **26**(47), 474205.
11 D. Xiang, X. Wang, C. Jia, *et al.*, Molecular-Scale Electronics: From Concept to Function, *Chem. Rev.*, 2016, **116**(7), 4318–4440.
12 J. A. Mol, C. S. Lau, W. J. M. Lewis, *et al.*, Graphene-porphyrin single-molecule transistors, *Nanoscale*, 2015, **7**(31), 13181–13185.
13 K. Ullmann, P. B. Coto, S. Leitherer, *et al.*, Single-Molecule Junctions with Epitaxial Graphene Nanoelectrodes, *Nano Lett.*, 2015, **15**(5), 3512–3518.
14 E. Burzurí, J. O. Island, R. Díaz-Torres, *et al.*, Sequential Electron Transport and Vibrational Excitations in an Organic Molecule Coupled to Few-Layer Graphene Electrodes, *ACS Nano*, 2016, **10**(2), 2521–2527.

15 T. Pei, J. O. Thomas, S. Sopp, *et al.*, Exchange-induced spin polarization in a single magnetic molecule junction, *Nat. Commun.*, 2022, **13**(1), 4506.
16 Z. Chen, J.-R. Deng, S. Hou, *et al.*, Phase-Coherent Charge Transport through a Porphyrin Nanoribbon, *J. Am. Chem. Soc.*, 2023, **145**(28), 15265–15274.
17 W. Niu, S. Sopp, A. Lodi, *et al.*, Exceptionally clean single-electron transistors from solutions of molecular graphene nanoribbons, *Nat. Mater.*, 2023, **22**(2), 180–185.
18 Y. Cao, S. Dong, S. Liu, *et al.*, Building High–Throughput Molecular Junctions Using Indented Graphene Point Contacts, *Angew. Chem., Int. Ed.*, 2012, **51**(49), 12228–12232.
19 C. Jia and X. Guo, Molecule–electrode interfaces in molecular electronic devices, *Chem. Soc. Rev.*, 2013, **42**(13), 5642.
20 Q. Xu, G. Scuri, C. Mathewson, *et al.*, Single Electron Transistor with Single Aromatic Ring Molecule Covalently Connected to Graphene Nanogaps, *Nano Lett.*, 2017, **17**(9), 5335–5341.
21 P. Puczkarski, P. Gehring, C. S. Lau, *et al.*, Three-terminal graphene single-electron transistor fabricated using feedback-controlled electroburning, *Appl. Phys. Lett.*, 2015, **107**(13), 133105.
22 J. Moser and A. Bachtold, Fabrication of large addition energy quantum dots in graphene, *Appl. Phys. Lett.*, 2009, **95**(17), 173506.
23 A. Barreiro, H. S. J. van der Zant and L. M. K. Vandersypen, Quantum Dots at Room Temperature Carved out from Few-Layer Graphene, *Nano Lett.*, 2012, **12**(12), 6096–6100.
24 P. Recher, J. Nilsson, G. Burkard, *et al.*, Bound states and magnetic field induced valley splitting in gate-tunable graphene quantum dots, *Phys. Rev. B: Condens. Matter Mater. Phys.*, 2009, **79**(8), 085407.
25 S. Schnez, F. Molitor, C. Stampfer, *et al.*, Observation of excited states in a graphene quantum dot, *Appl. Phys. Lett.*, 2009, **94**(1), 012107.
26 R. K. Puddy, C. J. Chua and M. R. Buitelaar, Transport spectroscopy of a graphene quantum dot fabricated by atomic force microscope nanolithography, *Appl. Phys. Lett.*, 2013, **103**(18), 183117.
27 D. Bischoff, A. Varlet, P. Simonet, *et al.*, Localized charge carriers in graphene nanodevices, *Appl. Phys. Rev.*, 2015, **2**(3), 031301.
28 J. Shen, Y. Zhu, X. Yang, *et al.*, Graphene quantum dots: emergent nanolights for bioimaging, sensors, catalysis and photovoltaic devices, *Chem. Commun.*, 2012, **48**(31), 3686.
29 B. Limburg, J. O. Thomas, G. Holloway, *et al.*, Anchor Groups for Graphene–Porphyrin Single–Molecule Transistors, *Adv. Funct. Mater.*, 2018, **28**(45), 1803629.
30 J. G. Simmons, Generalized Formula for the Electric Tunnel Effect between Similar Electrodes Separated by a Thin Insulating Film, *J. Appl. Phys.*, 1963, **34**(6), 1793–1803.
31 C. C. Escott, F. A. Zwanenburg and A. Morello, Resonant tunnelling features in quantum dots, *Nanotechnology*, 2010, **21**(27), 274018.
32 E. A. Osorio, T. Bjørnholm, J. M. Lehn, *et al.*, Single-molecule transport in three-terminal devices, *J. Phys.: Condens. Matter*, 2008, **20**(37), 374121.
33 B. Gelmont, M. S. Shur and R. J. Mattauch, Disk and stripe capacitances, *Solid-State Electron.*, 1995, **38**(3), 731–734.
34 Z. Ge, S. Slizovskiy, P. Polizogopoulos, *et al.*, Giant orbital magnetic moments and paramagnetic shift in artificial relativistic atoms and molecules, *Nat. Nanotechnol.*, 2023, **18**(3), 250–256.
35 P. Gehring, J. K. Sowa, J. Cremers, *et al.*, Distinguishing Lead and Molecule States in Graphene-Based Single-Electron Transistors, *ACS Nano*, 2017, **11**(6), 5325–5331.
36 S. Schnez, K. Ensslin, M. Sigrist, *et al.*, Analytic model of the energy spectrum of a graphene quantum dot in a perpendicular magnetic field, *Phys. Rev. B: Condens. Matter Mater. Phys.*, 2008, **78**(19), 195427.
37 M. O. Goerbig, Electronic properties of graphene in a strong magnetic field, *Rev. Mod. Phys.*, 2011, **83**(4), 1193–1243.
38 D.-K. Ki and A. F. Morpurgo, Crossover from Coulomb Blockade to Quantum Hall Effect in Suspended Graphene Nanoribbons, *Phys. Rev. Lett.*, 2012, **108**(26), 266601.
39 H. T. Man and A. F. Morpurgo, Sample-Specific and Ensemble-Averaged Magnetoconductance of Individual Single-Wall Carbon Nanotubes, *Phys. Rev. Lett.*, 2005, **95**(2), 026801.
40 J. Kong, E. Yenilmez, T. W. Tombler, *et al.*, Quantum Interference and Ballistic Transmission in Nanotube Electron Waveguides, *Phys. Rev. Lett.*, 2001, **87**(10), 106801.
41 D. Bischoff, F. Libisch, J. Burgdörfer, *et al.*, Characterizing wave functions in graphene nanodevices: Electronic transport through ultrashort graphene constrictions on a boron nitride substrate, *Phys. Rev. B: Condens. Matter Mater. Phys.*, 2014, **90**(11), 115405.

